We are IntechOpen, the world's leading publisher of Open Access books Built by scientists, for scientists

4,800
Open access books available

122,000
International authors and editors

135M
Downloads

Our authors are among the

154
Countries delivered to

TOP 1%
most cited scientists

12.2%
Contributors from top 500 universities

CLARIVATE ANALYTICS BOOK CITATION INDEX INDEXED

WEB OF SCIENCE™

Selection of our books indexed in the Book Citation Index in Web of Science™ Core Collection (BKCI)

Interested in publishing with us?
Contact book.department@intechopen.com

Numbers displayed above are based on latest data collected.
For more information visit www.intechopen.com

Chapter 5

Extreme Precipitation Events over East Asia: Evaluating the CMIP5 Model

Nicolas Freychet, Huang-Hsiung Hsu and Chi-Hua Wu

Additional information is available at the end of the chapter

http://dx.doi.org/10.5772/62996

Abstract

Extreme hydrological events are a direct threat to society and the environment, and their study within the framework of global climate change remains crucial. However, forecasts present numerous uncertainties.

This study investigates the modification of precipitation characteristics over East Asia, a region densely populated and vulnerable to extreme rainfall. The performance of the models and the confidence in their projections are analyzed using data derived from an ensemble of models from Phase 5 of the Coupled Model Intercomparison Project (CMIP5). Different factors that can affect the confidence of the projection are considered, such as the resolution, the response to radiative forcing, and the modification of large-scale atmospheric circulation.

The resolution and response in radiative forcing do not exhibit a clear correlation with the change in precipitation. The moisture flux convergence (MFC), by contrast, has a clear impact on extreme events. Specifically, the change in the dynamical term of the vertical MFC exhibits a major disagreement among the models and could strongly affect the confidence of the ensemble projection. Extreme precipitation is likely to increase over East Asia and India.

Keywords: Extreme precipitation, CMIP5, East Asia monsoon, RCP8.5, variability

1. Introduction

The Asian subcontinent is one of the most densely populated areas on the Earth and is also one of the most vulnerable regions to environmental conditions. The region is subject to

strong seasonal variations in precipitation, with wet summers and drier winters. The dynamics of the Asian summer monsoon have been reviewed in many papers [e.g., 1–5]. The monsoon provides necessary water for societal needs, but can also be associated with extreme precipitation. This type of rainfall represents a dual threat to society. First, the rain falls in excess amounts over a short period, resulting in a high runoff rather than recharging the groundwater supply. Second, extreme precipitation often leads to floods and, eventually, to landslides, building collapses, and causalities. Extreme precipitation in East Asia is often associated with typhoons, but it can also be triggered by other atmospheric conditions, such as a recent extreme rainfall event that occurred over China in the late spring and early summer of 2015. Heavy rainfall (above 60 mm day^{-1}) first affected the southern provinces before moving toward the central and northern parts of the country. Overall, several hundreds of thousands of people were affected, tens of thousands of houses were destroyed, several people died, and crops and roads were severely damaged.[1] These effects showcase the need for anticipating and planning hydrological extreme events, including answering the following question: How will global climate change affect the characteristics of extreme rainfall?

Various studies have investigated the projections of precipitation in a warming climate [6–19] and the modification of monsoon systems under such conditions [20–27]. The global and regional patterns of extreme rainfall changes have also been subject to research [28–36]. The Intergovernmental Panel on Climate Change Fourth Assessment Report (IPCCAR4) presents a summary of these studies; for example, Chapters 10.3.6 [37] and 11.4 [38] detail projections for Asia. However, one critical problem remains: To what extent can we trust the models? Phase 5 of the Coupled Model Intercomparison Project (CMIP5) provides a wide range of models, each with its own characteristics (e.g., parametrization and resolution). The study of an ensemble extracted from the CMIP5 is a good approach to investigating the uncertainties associated with the projection and to quantifying its confidence. In this study, 23 models are used, all in accordance with the representative concentration pathway 8.5 (RCP8.5), to answer the following questions: How will precipitation characteristics change over East Asia by the end of the twenty-first century? How reliable are these projections? What can explain the scattering of the ensemble? Moreover, what will be the social and economic impacts?

Section 2 details the data and methodology used. Section 3 introduces a review of the performance of the CMIP5 models as well as a comparison against observations and then an analysis on the estimated ensemble projection and its reliability. Section 4 presents a more detailed discussion on the change in atmospheric characteristics associated with the change in extreme rainfall. Section 5 provides a brief discussion on possible societal impacts, and Section 6 offers a conclusion.

[1] Statistics from: floodlist.com/tag/china

http://dx.doi.org/10.5772/62996

2. Data and methodology

2.1. Data

To examine the projection and reliability of the CMIP5 ensemble, 23 models (**Table 1**) are used (with a single member for each). The models were first forced by historical conditions (the observation of aerosols, greenhouse gases, and solar irradiance) until 2005 and then followed the RCP8.5 pathway [39], leading to an increase in radiative forcing of 8.5 W m^{-2} by the end of 2100. The projection of the ensemble is analyzed by conducting a comparison between the last 30 years of the century (i.e., from 2071 to 2100, called "RCP" hereafter) and 30 years of the historical period (i.e., from 1976 to 2005, called "HIST" hereafter). Extreme events are computed from the daily outputs, and then the results are averaged for the 30 years of each period.

Model Name	Institute and Country	Resolution
ACCESS1.0	Commonwealth Scientific and Industrial Research Organization (CSIRO), and Bureau of Meteorology (BoM), Australia	144 × 192
ACCESS1.3	CSIRO and BoM, Australia	144 × 192
BCC-CSM1.1	Beijing Climate Center (BCC) and China Meteorological Administration (CMA), China	64 × 128
BCC-CSM1.1(m)	BCC and CMA, China	160 × 320
BNU-ESM	Beijing Normal University (BNU)–Earth System Model, China	64 × 128
CanESM2	Canadian Centre for Climate Modeling and Analysis (CCCma), Canada	64 × 128
CMCC-CESM	Centro Euro-Mediterraneo per i Cambiamenti Climatici (CMCC), Italy	48 × 96
CMCC-CM	CMCC-CM, Italy	240 × 480
CMCC-CMS	CMCC-CM, Italy	96 × 192
CNRM-CM5	Centre National de Recherches Météorologiques (CNRM), and Centre Européen de Recherches et de Formation Avancée en Calcul Scientifique, France	128 × 256
CSIRO-Mk3–6-0	CSIRO Marine and Atmospheric Research (Melbourne) in collaboration with the Queensland Climate Change Centre of Excellence (QCCCE) (Brisbane)	96 × 192
FGOALS-G2	Institute of Atmospheric Physics, Chinese Academy of Sciences (IAP), and Tsinghua University (THU), China	60 × 128
GFDL-CM3	Geophysical Fluid Dynamics Laboratory (GFDL), USA	90 × 144
GFDL-ESM2G	GFDL, USA	90 × 144
GFDL-ESM2M	GFDL, USA	90 × 144
IPSL-CM5A-LR	Institut Pierre-Simon Laplace (IPSL), France	96 × 96
IPSL-CM5A-MR	IPSL, France	143 × 144

Model Name	Institute and Country	Resolution
IPSL-CM5B-LR	IPSL, France	96 × 96
MIROC5	Atmosphere and Ocean Research Institute (AORI; The University of Tokyo), National Institute for Environmental Studies (NIES), and Japan Agency for Marine-Earth Science and Technology (JAMSTEC), Japan	128 × 256
MIROC5-ESM-CHEM	JAMSTEC, AORI, and NIES, Japan	64 × 128
MPI-ESM-LR	Max Planck Institute for Meteorology (MPI-M), Germany	96 × 192
MRI-CGCM3	Meteorological Research Institute, Japan	160 × 320
NorESM1-M	Norwegian Climate Centre, Norway	96 × 144

Table 1. CMIP5 models used for this study. The resolution is indicated in grid points (latitude × longitude).

Asia covers a large area with different regional climatologies (**Figure 1**). The mean precipitation during the extended summer (May–August) season is computed from the daily (1997–2007) Global Precipitation Climatology Project (GPCP) observations [40]. The total domain is subdivided into three regions based on the different phases of the Asian summer monsoon: East Asian region (EAR: 22°–45°N, 105°–145°E), India region (IR: 5°–28°N, 70°–105°E), and the western North-Pacific region (WNPR: 5°–22°N, 105°–160°E). The results are averaged over each of the three subregions to compare the regional characteristics of the rainfall.

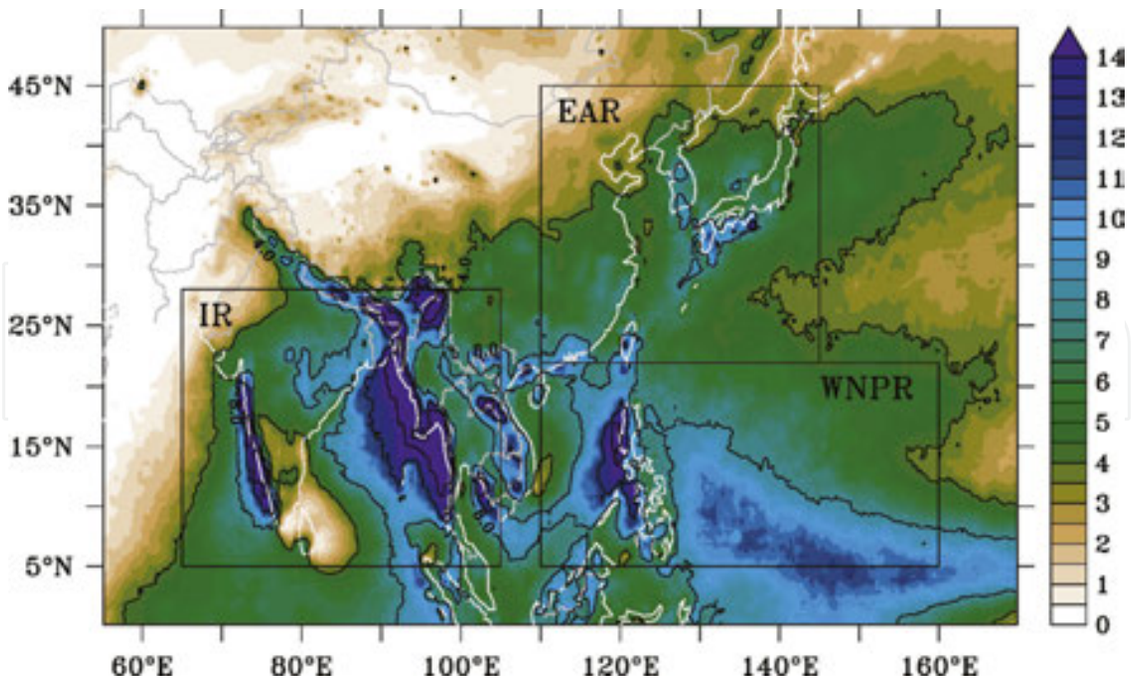

Figure 1. Mean May–August precipitation (mm day^{-1}) from GPCP [40] daily data (1997–2007), and an illustration of the three main domains used for this study: EAR(22°–45°N, 105°–145°E), IR(5°–28°N, 70°–105°E), and WNPR (5°–22°N, 105°–160°E).

http://dx.doi.org/10.5772/62996

2.2. Methodology

The overall methodology of this study follows that used in [41]. To study the characteristics of precipitation, the probability density function (pdf) is computed to separate and highlight the types of rainfall. Both intensity and frequency are considered and are defined as follows.

2.2.1. Intensity

Intensity is computed by separating the precipitation into percentiles at each grid point. Values are computed by steps of 10 between 1 and 90 and by steps of 1 between 90 and 99. Percentiles are computed either for the entire year (using all 30 years) or for each month (using only the precipitation from identical months over 30 years). The intensity of a percentile X is denoted as $pctX$ and is expressed in mm day^{-1}.

2.2.2. Frequency

Frequency indicates the occurrence of a certain range of precipitation. It is computed for each grid point by using a threshold based on the HIST intensity value of a yearly percentile (this threshold is therefore independent from the month) and averaged over a 10° × 10° box around this point. At each grid point, each day with rainfall higher than this threshold is counted as an event (for the given percentile). The HIST and RCP use the same threshold value for a percentile, and thus the same definition for light and heavy rainfall is used for both periods, which facilitates comparing the change in each percentile. The frequency is determined by averaging the count of events from the same months over 30 years. The frequency of a percentile X is denoted as $fqpctX$ and is expressed as a number of days.

The projection is expressed either as a difference between the two periods (RCP – HIST) or as a relative difference ([(RCP – HIST)/HIST] × 100). The former has a unit depending on the variable, whereas the relative difference is always expressed as a percentage. Each value was computed independently for every model on the respective grids. To plot the spatial distributions, the results were interpolated on a common grid (1.5° × 1.5°) to compute the ensemble mean and the associated ensemble standard deviation.

A change in intensity translates how each type of rainfall (light, medium, and heavy) could become more or less intense, while the change in frequency indicates how each type of rainfall could become more or less frequent.

3. Confidence in the distribution of precipitation and its projection

3.1. A brief review of the historical CMIP5 ensemble performances

First, the capability of the ensemble to simulate the precipitation and monsoon circulation over Asia is reviewed briefly. **Figure 2** shows the annual signal of precipitation in Asia for the 1976–2005 period (HIST) for the ensemble mean and the GPCP daily data (averaged over 1997–2007). The 99th percentile is also computed for each grid point over the entire period and then

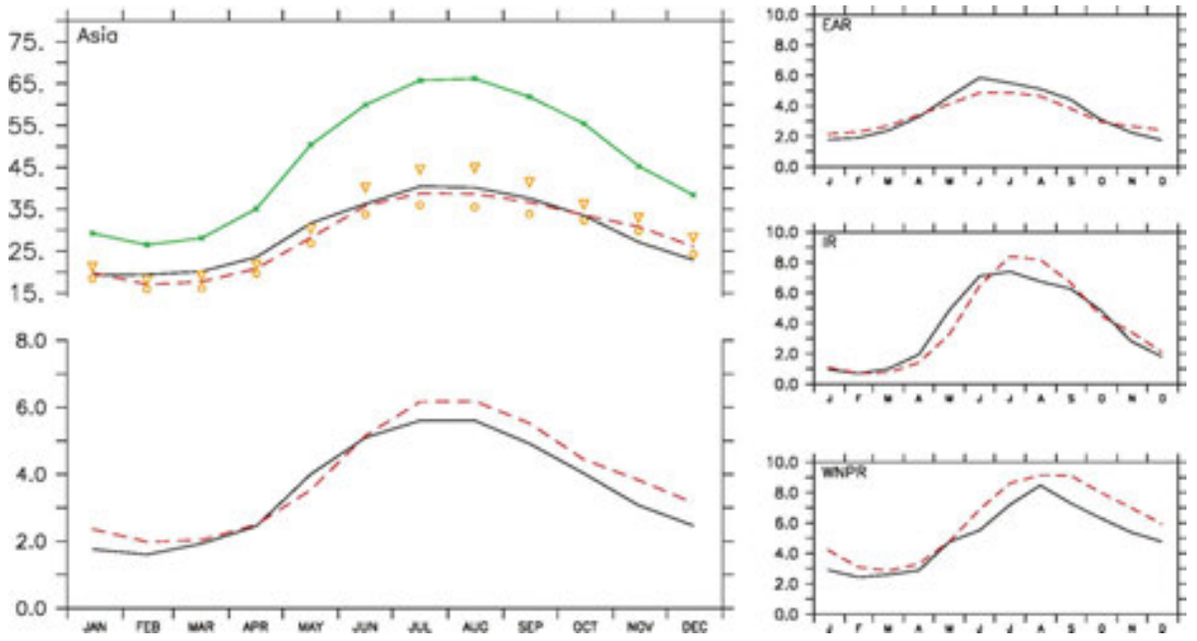

Figure 2. Annual signal of precipitation (mm day^{-1}) in the Asia region (5°–45°N, 65°–160°E), EAR (22°–45°N, 105°–145°E), IR (5°–28°N, 70°–105°E), and WNPR (5°–22°N, 105°–160°E). The solid black line represents the GPCP observations, and the dashed red line indicates the CMIP5 ensemble mean. For the Asia region (left), on the top panel, the solid black and dashed red lines indicate the 99th percentile for the GPCP and CMIP5, respectively, and the orange triangles (circles) correspond to the mean value of the 10 models with the highest (lowest) resolution. The PERSIANN observational dataset is also plotted for the 99th percentile (solid green line). The signal is averaged over 1976–2005 for the CMIP5 ensemble and 1997–2007 for the observations.

averaged for the Asia domain (5°–45°N, 65°–160°E). Another observational dataset is used for the 99th percentile (PERSIANN, [42]), which has a 0.25° resolution.

The mean signal of the ensemble is relatively consistent with observations, and it can detect the seasonal signal for each region, although it tends to overestimate (underestimate) the precipitation over WNPR (EAR) during the summer. A significant delay in the onset of the monsoon over IR is also visible. The signal of extreme precipitation (99th percentile) is also adequately represented in a comparison between the CMIP5 mean and the GPCP. However, the signal intensity is stronger with a higher-resolution dataset (PERSIANN). This impact of the resolution could also affect the individual model results. Thus, for the 99th percentile, we separated the 10 models with the highest resolution (triangles) and the 10 models with the lowest resolution (circles). The effect of the resolution is clearly apparent, establishing an increased estimation of the 99th intensity according to the highest-resolution models during the Asian summer monsoon (the triangles are closer to the observation line.).

Regarding the spatial distribution (**Figure 3**) for the mean precipitation and wind circulation, biases are more readily apparent. In this figure, two periods are separated to highlight the monsoon evolution: May–June (MJ) and July–August (JA). Overall, the mean circulation is adequately represented by the CMIP5 ensemble, as are the rainfall patterns, although the intensity of precipitation exhibits a low bias more clearly over the Mei-Yu front in the EAR (during MJ) and a negative (positive) bias over the northern (southern) part of the IR, partic-

http://dx.doi.org/10.5772/62996

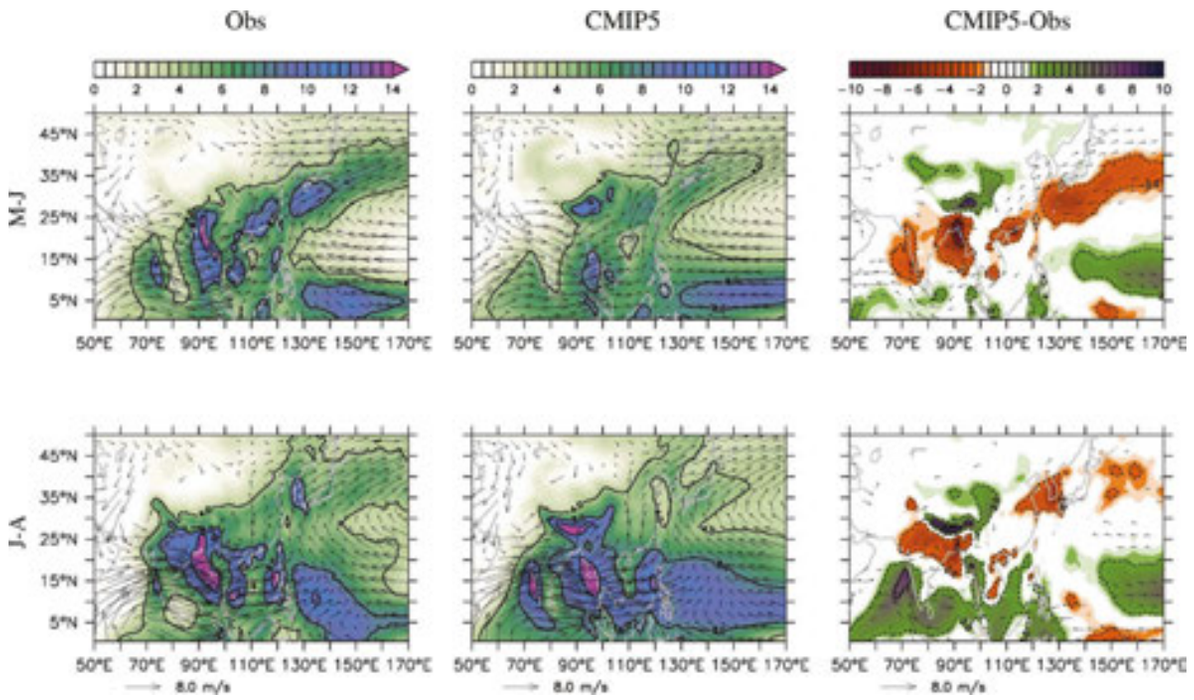

Figure 3. Climatology of the precipitation (shading) from the GPCP observations and the wind from the NCEP reanalysis (Obs); the CMIP5 ensemble mean (CMIP5) and the difference between the CMIP5 and the Obs. Two periods are separated: May–June (MJ) and July–August (JA). Intensity is in mm day^{-1} and contours are plotted every 4 mm day^{-1} for the Obs and CMIP5 and every 2 mm day^{-1} for the CMIP5-Obs.

ularly during JA. The underestimated precipitation resulted from unrealistic topography in the models, as indicated in [43]. A positive bias is observed over the WNPR and convective area. Thus, even if certain biases exist, the CMIP5 ensemble can reproduce the mean monsoon signal.

Finally, the distribution of extreme precipitation over Asia is shown in **Figure 4**. As shown in this figure, the occurrence of extreme events during the MJJA (top panel) is computed using the same threshold (pct99) based on the GPCP observations. This means that the models and observations were subject to the same criteria for identifying what is considered an extreme occurrence. The number of extreme events was then computed for each model (on its own grid), and the results were averaged for two groups: high- (CMIP HR, projected on a 1.5° × 1.5° grid) and low-resolution models (CMIP LR, projected on a 3° × 3° grid).

The location of extreme events is captured more accurately by the CMIP HR group, particularly where the topography is important (Himalayan plateau and Southeast Asia), but a stronger positive bias also occurs over the equatorial Pacific for this group. The CMIP LR can also represent the position of the main signals (west of India and the Bay of Bengal), but with less precision. This figure shows that the impact of resolution is critical for an accurate representation of extreme rainfall.

The tail end of the precipitation distribution is shown on the bottom panel for the individual models and the GPCP. The results are displayed for the three subregions. The resolution clearly

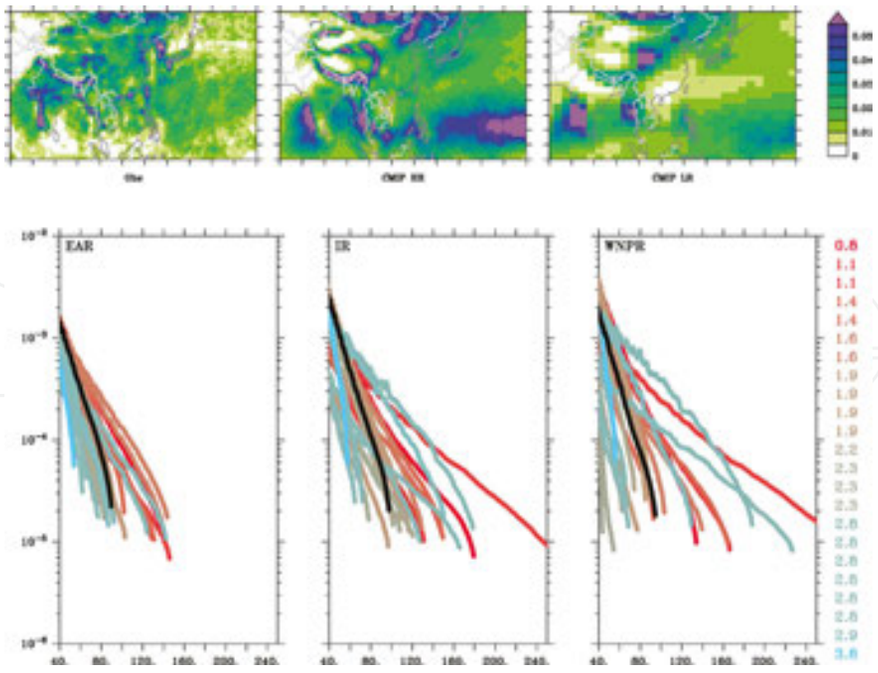

Figure 4. Climatology of extreme precipitation occurrence during the MJJA (top panel, in day month^{-1}) for the GPCP (Obs); 10 models each with the highest and lowest resolution (CMIP HR and CMIP LR, respectively). The bottom panel shows the tail end of the precipitation distribution computed from the GPCP (black) and from each model over each of the three subregions. Colors correspond to different resolutions, as indicated on the right-hand side of the panel.

affects the capacity of the model to produce more intense precipitation. Certain lower-resolution models (in blue) can also produce heavy rainfall; thus, the resolution is not always a limitation. Moreover, the ensemble is visibly more scattered over the WNPR and more consistent over the EAR. The confidence of the model ensemble can thus vary by region, which is a critical consideration when assessing the potential societal impacts in future climate projections.

These biases of the CMIP5 ensemble were examined in [44] and could significantly affect the reliability of the projection. Therefore, because of the systematic bias of the ensemble, the results of this study must be considered with a margin of error. If the bias is a supposed constant between the RCP and the HIST, a study of the change between the two periods should not be strongly affected; the difference between the periods should cancel out the bias.

3.2. Projected change in the distribution of the precipitation and its confidence

The ensemble projection of the precipitation characteristics for the end of the twenty-first century is investigated for each of the three subregions. The pdf of the precipitation is computed using a percentile method, and its projected change is plotted in **Figure 5**. The percentiles range from 1 (light precipitation) to 99 (extreme precipitation) and are grouped by tens between 1 and 90 and plotted sequentially between 90 and 99 so that the heaviest rainfall is highlighted in the figure. Both intensity and frequency are considered and plotted on separated panels, and each value is expressed as a relative change between the RCP and the

http://dx.doi.org/10.5772/62996

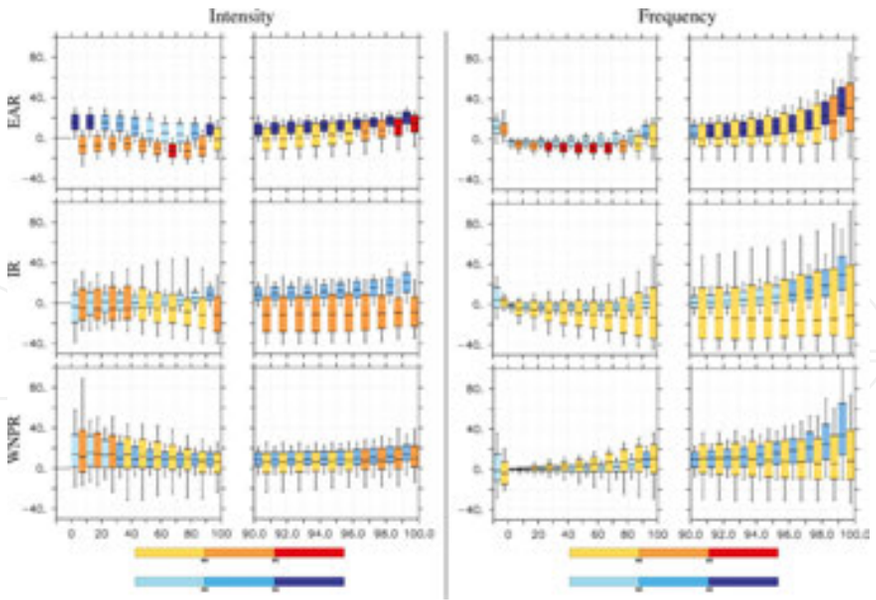

Figure 5. Probability density function (pdf) of the relative change (in percentages) in precipitation (left) intensity and (right) frequency. Precipitation is divided into 10 bins (from 1 to 100), and the last 10% is also divided into 10 bins of 1% each. Results are categorized between the wet season (blue charts) and dry season (orange charts) of each region. The colored boxes show the 25th–75th ensemble quantile, and the bars indicate the 10th–90th ensemble quantile. The horizontal black bars inside the boxes show the 50th ensemble percentile. In the frequency plots, the first bin (before 0) represents the dry days. The color scale indicates the values that exceeded a certain confidence level (90 or 95%) as computed from a Student's *t* test.

HIST (in percentages). To investigate the possible seasonal differences, the winter (December–March) and summer (May–August) periods are separated by color (blue for winter, and orange or red for summer). Finally, the signal of the dry days (defined as days with rainfall lower than the first percentile) is shown on the frequency plots before the 0 value.

One focus of this study is the reliability of the ensemble projection. Thus, for each bin, the 25th to 75th ensemble quartile intervals are indicated by colored boxes, and the 10th to 90th ensemble quartile intervals are indicated by black bars. The black horizontal bar inside the color chart represents the 50th ensemble percentile. To highlight the most significant results, the values that are significant at the 90% or 95% confidence level based on a Student's *t*-test are plotted with darker colors.

The results for the winter season, which is also the driest, are overall below the 90% confidence level. In the EAR, a dry tendency is clearly visible, with a confident decrease in frequency and intensity for the medium precipitation. This behavior is also visible for the intensity in the IR, but with a lower confidence level.

During the wet season (summer), when extreme rainfall occurs, all ranges of precipitation increase in all subregions, particularly for the heaviest rainfall (above the 90th percentile). For this type of precipitation, the confidence is higher (compared with medium to light precipitation), particularly for the EAR results. When examining the most extreme precipitation (the 99th percentile), almost all models are in agreement regarding the tendency to increase (the

10th ensemble percentile being above or near 0), although the magnitude of augmentation varies (from slightly more than 0 to 100%).

These results clearly indicate the threat that global warming could pose to the East Asian region. The most confident changes indicate an increase in extreme precipitation everywhere during the summer and a possible decrease in medium precipitation during the winter. The EAR region has the highest confidence levels (for both summer and winter), and thus the region will undeniably, at a minimum, be challenged by severe hydrological threats. At present, it is also clear that major uncertainties remain. The ensemble projections are scattered, particularly over the WNPR and IR regions, and uncertainties associated with ensemble projections over these regions were previously examined [45]. Many factors could affect ensemble scattering, such as parametrization schemes, the resolution, the response in radiative forcing, or the response in terms of atmospheric circulation. Most of these possibilities are explored in subsequent sections.

4. Intensification of the extremes during the summer monsoon: a change in atmosphere dynamics?

In this section, potential factors that could explain the scattering of the ensemble projection are investigated.

4.1. Impact of the resolution and radiative forcing

A part of the uncertainty could be due to the response of the surface temperature to the increase in radiative forcing in the models. Certain models revealed only a weak increase in temperature, which could explain the lower increase in (extreme) precipitation. To investigate this hypothesis, the changes in extreme precipitation characteristics versus the changes in surface temperature (averaged over the globe) in each model during the wet season is plotted in **Figure 6** (right-hand side).As mentioned in [41], the results do not exhibit a significant correlation between the response in surface temperature in the models and the change in extreme precipitation (intensity or frequency), although the strongest frequency increase is reached mostly by the models with a stronger increase in temperature.

Another factor that may affect the projection is the model resolution. Section 3.1 presented a significant relationship between the horizontal resolution and the capacity of the models to simulate heavy rainfall. When considering the change (left-hand side of **Figure 6**), the relationship between the resolution and the change of extreme events are nonsignificant. This result is also supported when examining the spatial distribution of the change in extreme occurrences for each model (**Figure 7**). The model of the same category (high or low resolution) can clearly produce conflicting signals. However, high-resolution models tend to have a stronger response, particularly over the equatorial oceanic region. A higher sensitivity in high-resolution models (particularly in convection) to changes in the environment at a small spatial scale may explain this stronger signal.

http://dx.doi.org/10.5772/62996

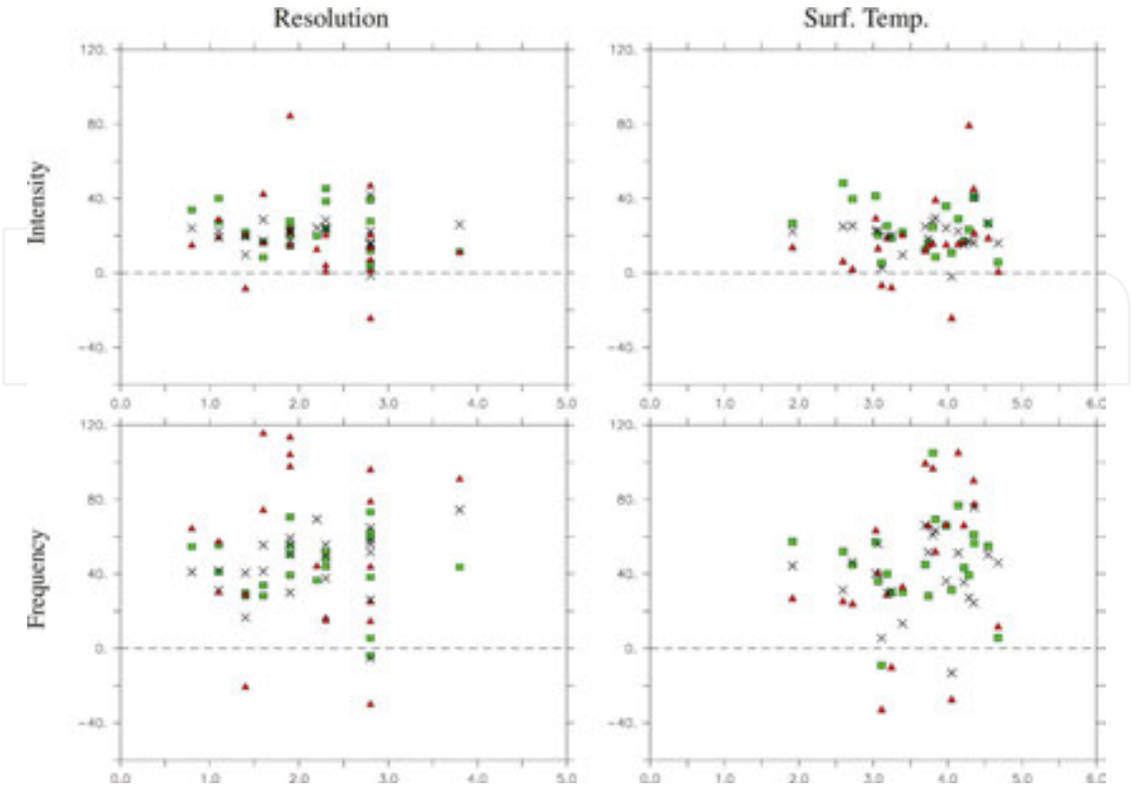

Figure 6. Scatterplots of the relative change during the wet season (for each model) in extreme precipitation (y axis, in percent) intensity (top) and frequency (bottom) versus the change in surface temperature (right, °C) and the mean resolution of each model (left). Black crosses, green squares, and red triangles, respectively, indicate the EAR, IR, and WNPR.

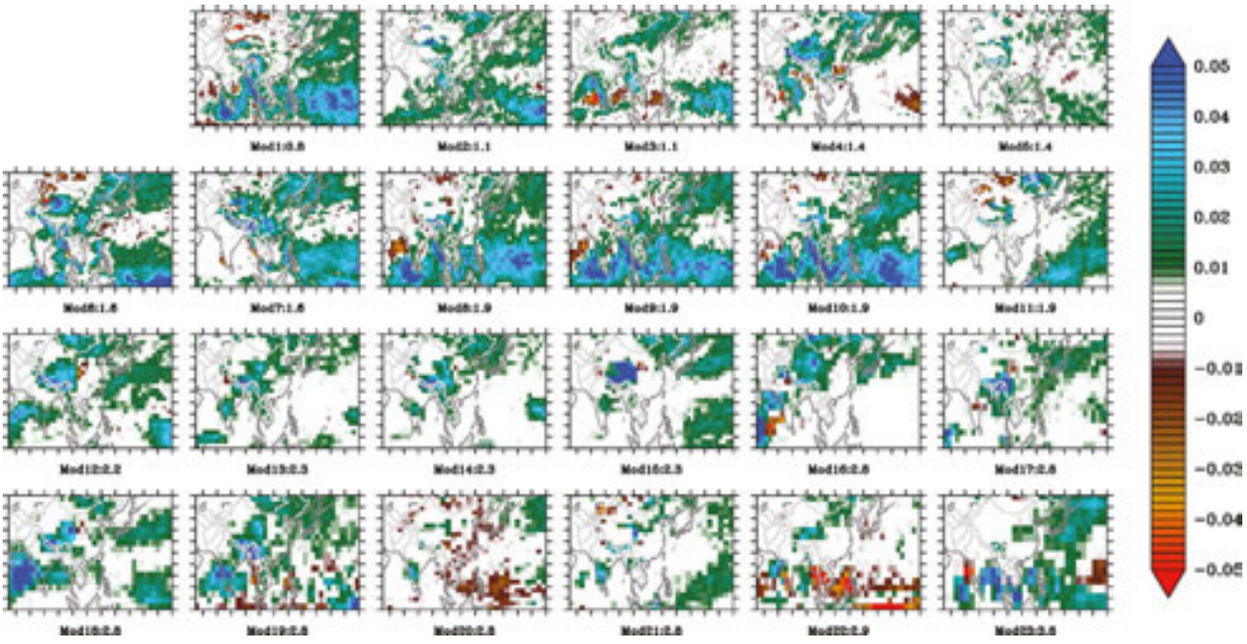

Figure 7. Change in the occurrence of extreme rainfall (day month^{-1}) for each model during the MJJA.

Based on these results, the resolution and the response to the radiative forcing are concluded not to be the main factors affecting the scattering of the ensemble projection and thus the reliability. The following subsection emphasizes the change in the circulation characteristics and its impact on rainfall projection.

4.2. Change in mean atmospheric circulation

4.2.1. Monthly mean circulation

The Asian summer monsoon is characterized by many active phases and short breaks, which can affect the precipitation characteristics. The results are summarized for two averaged periods: May–June (late spring) and July–August (summer). The late spring period corresponds with the onset of the global monsoon system and is also the main active phase for the Mei-Yu front system that develops over the EAR region. By contrast, the summer season corresponds with the main active phase of the monsoon over the IR and WNPR regions before decreasing in late summer.

The change in mean circulation in the low-level atmosphere (850 hPa) is displayed in **Figure 8** for the early spring and summer periods. The change in wind is indicated by the vectors, and the change in moisture flux (MF) is shown by the color shading. For the MF, only the values that exceeded a 90% confidence level with a Student's *t* test are shaded. During both phases, the MF and wind strengthen north of the IR region and along the east coast of Asia. The wind intensity is also decreased south of the IR region, but the change in MF is nonsignificant in this area. The MF results are not statistically significant over oceanic areas, particularly for the WNPR region. Despite good agreement between the models regarding an increase in atmospheric moisture content (data not shown), the change in MF for these areas is unclear (less than the 90% confidence level), meaning that the main uncertainties for the MF is caused by wind variations.

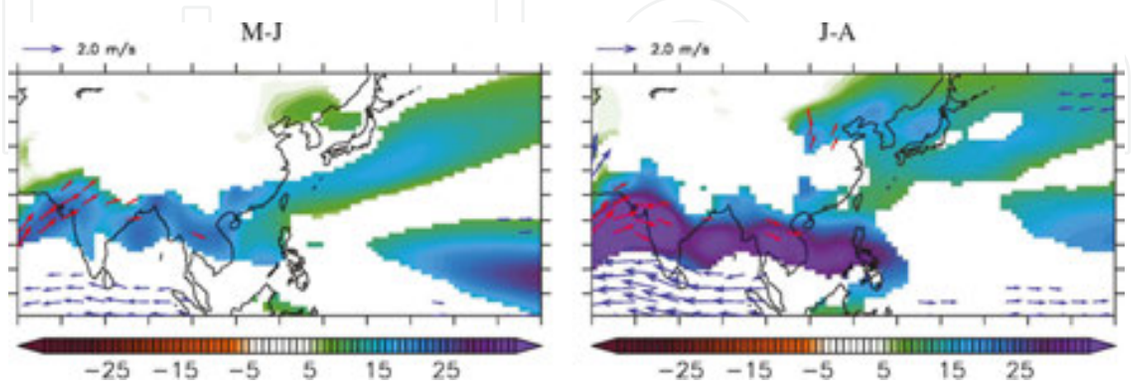

Figure 8. Change in 850 hPa moisture flux (shading, g kg^{-1} m s^{-1}) and winds (vectors, m s^{-1}), averaged over MJ and JA. For the winds, the vectors are plotted only for a change larger than 0.5 m s^{-1}, and red (blue) indicates positive (negative) changes. For the moisture flux, only values that exceeded a 90% confidence level with a two-tailed Student's *t* test are shaded.

http://dx.doi.org/10.5772/62996

The changes observed for low-level circulation appear to favor the triggering of heavy rainfall by increasing the moisture transport along South and East Asia. However, extreme events are typically associated with deep convection, affecting the entire troposphere. Thus, to gain an improved view of the change in atmospheric circulation, the change in MF convergence is computed for each layer of the atmosphere. Its correlation with the change in extreme rainfall is examined in the next section.

4.2.2. Daily horizontal moisture flux convergence

The horizontal MF convergence (HMFC) is expressed here as the sum of the contributions of a convergence term, the HMFCt (Eq. 1), and an advection term, the HMFCd (Eq. 2). The total MF convergence is obtained by summing the first two equations (Eq. 3). For Equations 1–3, q is the relative humidity, and u and v represent the zonal and meridional components of the wind, respectively. The specific contribution of the surface flux is not examined here, but it is implicitly included in the atmospheric humidity content. The changes in the HMFC profile and its two terms during the summer are separated, as shown in **Figure 9** (averaged over Asia). The correlation between the change in each term and that in the extreme precipitation characteristics is also computed over each subregion (**Figure 10** and **Table 2**). The correlations are based on individual model results, and the changes in the HMFC and its two components are averaged for the 200–850 hPa atmospheric levels. Results with values exceeding the 99% confidence level are indicated in bold.

$$\mathrm{HMFCt} = -\mathrm{q}\left[\left(\frac{\partial \mathrm{u}}{\partial \mathrm{x}}\right)+\left(\frac{\partial \mathrm{v}}{\partial \mathrm{y}}\right)\right] \tag{1}$$

$$\mathrm{HMFCd} = -\mathrm{u}\left[\left(\frac{\partial \mathrm{q}}{\partial \mathrm{x}}\right)\right]-\mathrm{v}\left[\left(\frac{\partial \mathrm{q}}{\partial \mathrm{y}}\right)\right] \tag{2}$$

$$\mathrm{HMFC} = \mathrm{HMFCt} + \mathrm{HMFCd} \tag{3}$$

The change in the HMFC is not statistically significant (**Figure 9**). The model ensemble scattering is large in each region and for each HMFC component. Determining a clear tendency is thus difficult, even when averaging the ensemble (red lines). However, **Figure 10** and the correlation coefficients in **Table 2** show that a clear relationship does not exist between the change in the HMFC and in either the intensity or frequency of extreme events. A significant correlation is found only for the change in the frequency of extremes over the WNPR (0.58 for HMFC and HMFCd). Thus, because the scattering of the change in MF convergence over this region is large, it may also significantly affect the scattering of the change in the extreme precipitation formation and thus the confidence of the projection. This does not apply to the other subregions.

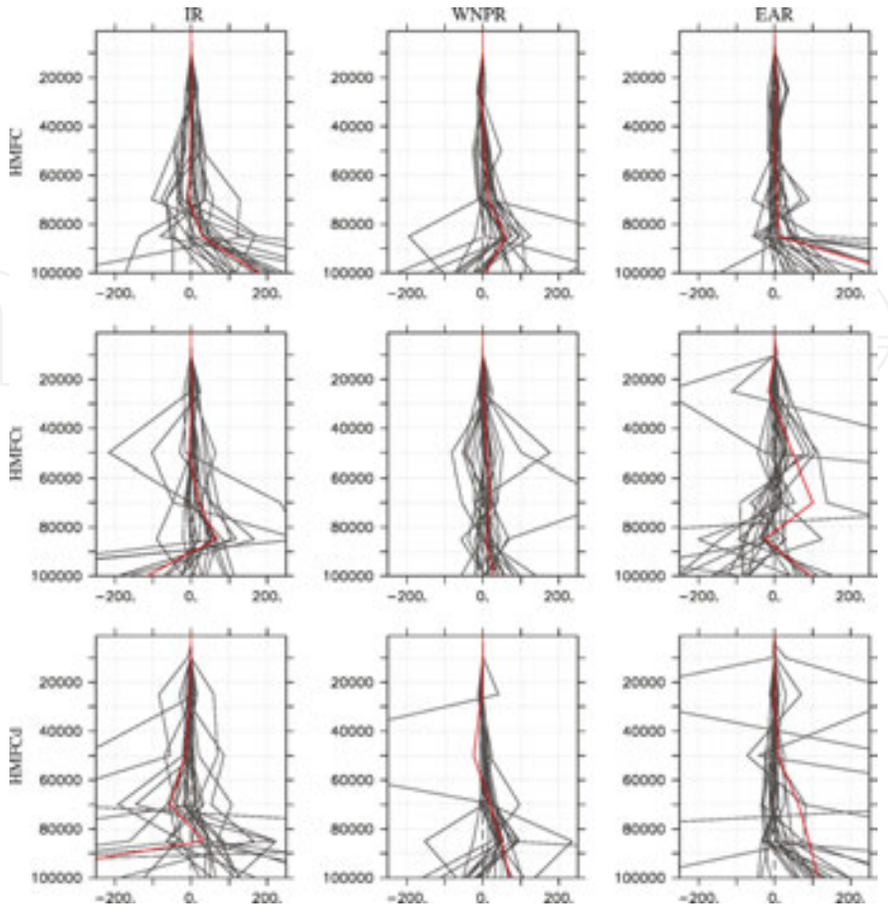

Figure 9. Relative change (in percentages) of (top) the HMFC profile and its (middle) convergence and (bottom) advection parts. Each change is normalized according to its mean historical value of the total atmospheric column (850–100 hPa). Black lines indicate separate models, and the red line represents the ensemble mean. The vertical axis indicates the pressure levels (in hPa). The scale is similar for each caption.

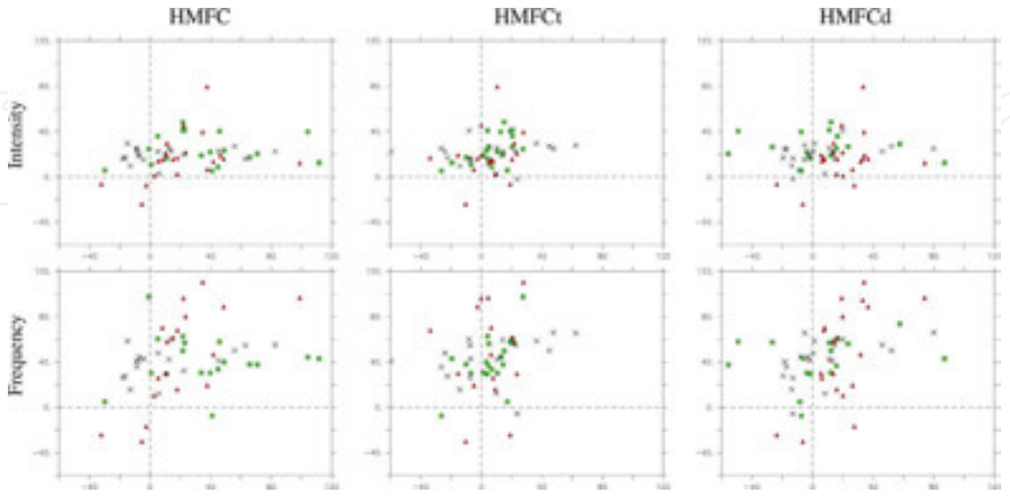

Figure 10. Similar to Figure 6, except for the change in the HMFC, HMFCt, and HMFCd versus that in the intensity and frequency of extreme precipitation.

http://dx.doi.org/10.5772/62996

Based on these results, the changes in horizontal circulation and convergence poorly affect the results of the extreme projections, except over the WNPR. The next section focuses on the change in vertical convergence.

	Intensity			Frequency		
	HMFC	**HMFCt**	**HMFCd**	**HMFC**	**HMFCt**	**HMFCd**
IR	0.04	0.22	−0.12	0.17	0.04	0.28
WNPR	0.26	0.11	0. 33	**0.58**	0.12	**0.58**
EAR	0.14	−0.01	0.16	0.25	0.1	0.33

Bold text indicates values exceeding the 99% confidence level.

Table 2. Linear correlation coefficients between the relative change in extreme precipitation (intensity and frequency) and in the HMFC (200–850 hPa) during the wet season (MJJA), separated into its convergence (HMFCt) and advection (HMFCd) parts.

4.3. Change in vertical circulation

This section has the same structure as Section 4.2.2, but discusses the vertical convergence. The vertical moisture convergence (VMFC) is defined as Eq. 4, with ω being representing the vertical velocity, $d_{p®}q$ representing the vertical gradient of a specific humidity, and the brackets indicating vertical integration. This is the most dominant term of the column-integrated moisture budget, particularly for heavy precipitation. The change in the VMFC is separated between the contributions of the thermodynamic term (*q*) and the dynamic term (ω).

$$VMFC = \langle \omega . d_{P®} q \rangle \tag{4}$$

The change in the VMFC profile and its two terms during the summer are shown in **Figure 11** (averaged over Asia). The correlation between the change in the VMFC and that in extreme events is displayed in **Figure 12**; the coefficients are listed in **Table 3**.

In contrast with the HMFC, the change in the VMFC is more apparent (**Figure 11**), although the scattering of the ensemble remains large, particularly for the IR and WNPR. The mean VMFC increases in each region (20–40%), particularly in the mid-troposphere. The VMFCt exhibits the same behavior, with a high confidence level (because of the expected increase in moisture in a warmer climate) and a higher magnitude in the low levels (40%). By contrast, the VMFCd is less certain, with a larger scattering and a mean closer to 0%. The change in the VMFCd tends to be negative and to oppose the positive change in the VMFCt. In summary, vertical convergence is expected to increase over each region, mostly because of the change in atmospheric moisture content, whereas the change in dynamics tends to increase the scattering of the ensemble (i.e., the uncertainties).

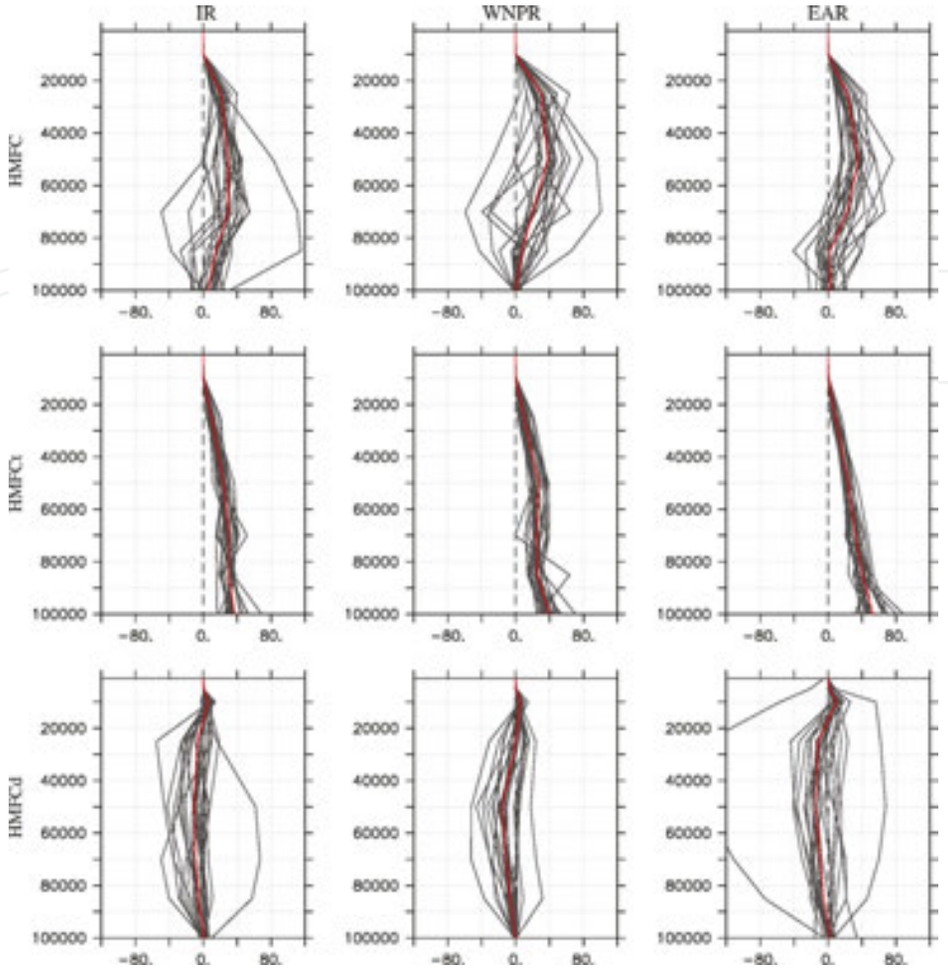

Figure 11. Similar to Figure 9 but for the VMFC, VMFCt, and VMFCd.

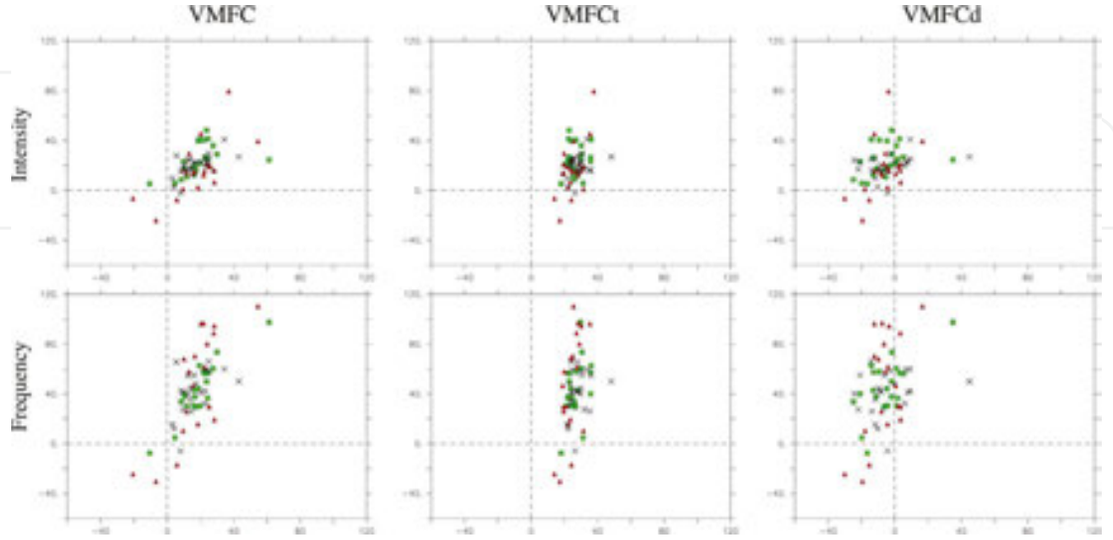

Figure 12. Similar to Figure 10 but for the VMFC, VMFCt, and VMFCd.

http://dx.doi.org/10.5772/62996

The correlations are also more apparent in **Figure 12** and **Table 3**, particularly for the total change in the VMFC. The changes in extreme precipitation characteristics are strongly correlated to the change in the VMFC (0.50–0.89). When considered separately, the correlation between the individual terms (VMFCt and VMFCd) with the changes in extreme precipitation become less clear. This is particularly applicable to the EAR, where significant correlations are found only for the total VMFC. The VMFCt significantly affects the WNPR in both frequency (0.75) and intensity (0.61), and the VMFCd is correlated with the frequency of extreme precipitation over the IR (0.63). These results clearly revealed that the change in extreme precipitation, both in frequency and intensity, is strongly affected by the change in the VMFC, and mostly under the simultaneous consideration of thermodynamic and dynamic terms.

	Intensity			**Frequency**		
	VMFC	**VMFCt**	**VMFCd**	**VMFC**	**VMFCt**	**VMFCd**
IR	**0.50**	0.12	0.33	**0.89**	0.41	**0.63**
WNPR	**0.67**	**0.61**	0.46	**0.72**	**0.75**	0.46
EAR	**0.67**	0.3	0.02	**0.51**	0.26	−0.14

Bold text indicates values exceeding the 99% confidence level.

Table 3. Identical to **Table 2**, except for vertical moisture flux convergence (VMFC) and its thermodynamical (VMFCt) and dynamical (VMFCd) components.

As mentioned in [41], these results may at first be contrary to expectations, which might anticipate an increase in atmospheric humidity content to be the dominant factor for explaining the change in extreme precipitation. The present research shows that the dynamical part of the VMFC can also significantly influence the intensity and frequency of these events. Furthermore, because its change is less apparent (**Figure 11**), it negatively influences confidence levels in projecting extremes (by increasing the scattering of the ensemble). By contrast, the change in the VMFCt is clearer and tends to increase confidence levels in projecting extremes.

4.4. Summary

In a warming climate, the specific humidity of the atmosphere is typically expected to increase. The variation in monsoon areas and precipitation has been linked to a rise in moisture convergence, offset by the change in circulation [15]. The earlier sections showed that the VMFC exerts a potentially high level of influence on the trends of extreme events, whereas the correlation between the change in the mean circulation and the HMFC is less clear. However, the influence of the VMFC varies significantly between regions, which is consistent with findings in [46], showing that the dynamic contribution induces spatial variations in the changes. The confidence of ensemble-projected change in extreme precipitation may clearly be influenced by the low level of agreement in the model dynamics, particularly in the IR and WNPR. A direct correlation was not found between the resolution of the models or their

response to radiative forcing and the change in extreme events, at least with the ensembles used for this study.

5. Extreme precipitation projections and societal impacts

These findings highlight the importance of considering regional studies when examining long-term projections of precipitation characteristics. Because of the different responses of the models to radiative forcing (in atmospheric circulation), the change in precipitation can be uncertain. However, the clearest and strongest tendencies are observed for heavy and extreme precipitation, which is also the most critical in terms of constituting a threat to society (but not for water resources, which is another subject of concern). Moreover, the regions for which the changes are most significant for these events are also those that are the most densely populated: East Asia and South Asia. Over these two regions, heavy rainfall is expected to increase in frequency and intensity with good confidence.

Considering past events (such as the floods of 2011, 2013, or 2015 that affected South Asia and China) and their cost, extreme hydrological events represent a severe threat to the populations living in these regions [47, 48]. It is most likely that the loss associated with these events (in terms of economy, infrastructure, land, and casualties) will increase by the end of the century. However, even if an increase in heavy rainfall cannot be avoided, its impact can be limited [49]. For instance, because deforestation is a major cause of landslides under heavy rainfall [50], improved management over forests could locally limit the impact of heavy rainfall [51]. In urban areas, drainage systems and infiltration surfaces can be improved to convey more surface water, as indicated in [52], which compared measurements conducted in various cities. Thus, if measures are considered and implemented sufficiently early, it is possible to limit the impact of heavy rainfall and its associated costs.

6. Discussion and concluding remarks

The change in extreme precipitation under global warming conditions will remain a major subject of research for the next few decades. Extreme precipitation events can drastically affect society, entailing severe economic, infrastructure, and human loss. The use of a model ensemble is a beneficial approach to highlighting regions where a change in these events is clear or, alternatively, regions where the level of agreement is lower. The frequency of extreme precipitation and the confidence level of the projected changes are critical considerations for decision makers in developing the prevention and risk management measures.

This study used 23 models from the CMIP5. Certain projections of precipitation characteristics can be clearly identified as confident, whereas other results remain uncertain (**Figure 5**). The selected models revealed a high confidence level in indicating that the East Asian region will be highly vulnerable to global warming, exhibiting more intense and more frequent extreme precipitation. The India and South Asian regions exhibit the same tendency but with less

confidence. The results in the western North Pacific region are less certain, particularly regarding the intensity of extremes. These findings are in agreement with those presented in [41], even if the ensemble used was different. Changes in the precipitation characteristics are likely to affect all Asian regions, but not with the same magnitude.

Different factors that can affect the scattering of the ensemble projection were studied through correlation analysis. The resolution of the models does not display a clear impact, although we found that it can significantly affect the capacity of the models to produce heavy rainfall (**Figure 4**). The response of the models to radiative forcing did not exhibit a clear relationship with the change of extremes (**Figure 6**). The most significant findings were obtained by considering daily moisture convergence over the entire atmosphere (Figures 9–12 and Tables 2 and 3). The vertically integrated moisture gradient can strongly influence the projection of extreme events. Specifically, the model results were not in agreement with the change of its dynamical term (VMFCd), and thus this may explain the uncertainties associated with the projection. Thus, even if the increase in atmospheric moisture content is expected to strengthen the precipitation, local variations in the circulation will strongly affect changes in the characteristics of extreme events.

The systematic bias of the CMIP5 models mentioned in Section 3, their low-level ability to simulate tropical cyclones correctly (with a resolution coarser than 1°), and the definition of the MF adopted herein could also lead to a biased estimation of the correlations computed for this study. Thus, the results should be considered indicators of what can affect the projection of extreme precipitation and ensemble uncertainties. However, other factors could also influence the response of the models and should be investigated in future studies. Nevertheless, most of the results indicate a confident increase in extreme precipitation over East Asia. The societal and economic impacts are expected to be massive, and anticipation will be critical to limiting the damage of such changes in hydrological events.

Acknowledgements

This work was supported by the Consortium for Climate Change Study (CCliCS) - Ministry of Science and Technology (MOST), Taiwan, under Grant MOST 100-2119-M-001-029-MY5. We thank the reviewers and editor for comments that greatly improved the manuscript.

Author details

Nicolas Freychet*, Huang-Hsiung Hsu and Chi-Hua Wu

*Address all correspondence to: nfreychet@gate.sinica.edu.tw

Research Center for Environmental Changes, Taipei, Taiwan

References

[1] Ramage CS. Monsoon Meteorology, International Geophysical Series, Vol. 15. Academic Press; 1971, San Diego. 296 p.

[2] Ding Y. The variability of the Asian summer monsoon. In: Kluwer Academic, editor. Monsoon over China. J. Meteor. Soc. Japan; 1994, pp. 85B, 21-54. DOI: 10.2151/jmsj.85B.21

[3] Chang C-P, Wang B, Lau N-C G. The global monsoon system: research and forecast. WMO/TD 1266, TMPRRep. 70 ed. 2005. 542 p.

[4] Wang B. The Asian Monsoon. Praxis Publishing; 2006, Chichester, UK. 787 p.

[5] Ding Y. The variability of the Asian summer monsoon. J. Meteor. Soc. Japan. 2007;85B: 21-54. DOI: 10.2151/jmsj.85B.21

[6] Chou C, Neelin J D. Mechanism of global warming impacts on regional tropical precipitation. J. Climate. 2004;17:2688–2701. DOI: 10.1175/1520-0442(2004)017,2688:MOGWIO.2.0.CO;2

[7] Min S-K, Legutke S, Hense A, Cubasch U, Kwon W-T, Oh J-H, Schlese U.. East Asian climate change in the 21st century as simulated by the coupled climate model ECHO-G under IPCC SRES scenarios. J. Meteor. Soc. Japan. 2006;84:1-26. DOI: 10.2151/jmsj.84.1

[8] Kripalani RH, Oh J-H, Chaudhari HS. Response of the East Asian summer monsoon to doubled atmospheric CO2: coupled climate model simulations and projections under IPCC AR4. Theor. Appl. Climatol. 2007;87:1-28. DOI: 10.1007/s00704-006-0238-4

[9] Stephens GL, Ellis TD. Controls of global-mean precipitation increases in global warming GCM experiments. J. Climate. 2008;21:6141-6155. DOI: 10.1175/2008JCLI2144.1

[10] Chou C, Neelin J D, Chen C-A, Tu J-Y. Evaluating the "rich-get-richer" mechanism in tropical precipitation change under global warming. J. Climate. 2009;22:1982–2005. DOI: 10.1175/2008JCLI2471.1

[11] Wu C-H, Kau W-S, Chou M-D. Summer monsoon onset in the subtropical western North Pacific. Geophys. Res. Lett. 2009;36:L18810. DOI: 10.1029/2009GL040168

[12] Seager R, Naik N, Vecchi GA. Thermodynamic and dynamic mechanisms for large-scale changes in the hydrological cycle in response to global warming. J. Climate. 2010;23:4651-4668. DOI: 10.1175/2010JCLI3655.1

[13] Chou C, Chen C-A, Tan P-H, Chen K-T. Mechanisms for global warming impacts on precipitation frequency and intensity. J. Climate. 2012;25:3291-3306. DOI: 10.1175/JCLI-D-11-00239.1

[14] Kusunoki S, Arakawa O. Change in the precipitation intensity of the East Asian summer monsoon projected by CMIP3 models. Climate Dyn. 2012;38:2055-2072. DOI: 10.1007/s00382-011-1234-7

[15] Hsu P-C, Li T, Luo J-J, Murakami H, Kitoh A, Zhao M. Increase of global monsoon area and precipitation under warming: a robust signal? Geophys Res Lett. 2012;39:L06701. DOI: 10.1029/2012GL051037

[16] Ma J, Xie S-P, Kosaka Y. Mechanisms for tropical tropospheric circulation change in response to global warming. J Climate. 2012;25:2979-2994. DOI: 10.1175/JCLI-D-11-00048.1

[17] Wu C-H, Chou M-D. Upper-tropospheric forcing on late-July monsoon transition in East Asia and western North Pacific. J Climate. 2012;25:3929-3941. DOI: 10.1175/JCLI-D-11-00343.1

[18] Seo, K-H, Ok J, Son J-H, Cha D-H. Assessing future change in the East Asian summer monsoon using CMIP5 coupled models. J Climate. 2013;26:7662-7675. DOI: 10.1175/JCLI-D-12-00694.1

[19] Lee J-Y, Wang B. Future change of global monsoon in the CMIP5. Climate Dyn. 2014;42:101-119. DOI: 10.1007/s00382-012-1564-0

[20] Wang B, Ding Q. Changes in global monsoon precipitation over the past 56 years. Geophys Res Lett. 2006;33:L06711. DOI: 10.1029/2005GL025347

[21] Inoue T, Ueda H. Delay of the first transition of Asian summer monsoon under global warming condition. SOLA. 2011;7:081-084. DOI: 10.2151/sola.2011-021

[22] Min S-K, Legutke S, Hense A, Cubasch U, Kwon W-T, Oh J-H, Schlese U. Projected changes in Asian summer monsoon in RCP scenarios of CMIP5. Atmos. Oceanic Sci Lett. 2012;5:43-48.

[23] Turner AG, Annamalai H. Climate change and the South Asian summer monsoon. Nat Climate Change. 2012;2:587-595. DOI: 10.1038/nclimate1495

[24] Duan A, Hu J, Xiao Z.. The Tibetan Plateau summer monsoon in the CMIP5 simulations. J Climate. 2013;26:7747-7766. DOI: 10.1175/JCLI-D-12-00685.1

[25] Hsu P-C, Li T, Luo J-J, Murakami H, Kitoh A, Zhao M. Increase of global monsoon area and precipitation under global warming: A robust signal? Geophys Res Lett. 2012;39:L06701. DOI: 10.1029/2012GL051037

[26] Jones C, Carvalho LMV. Climate change in the South American monsoon system: Present climate and CMIP5 projections. J Climate. 2013;26:6660-6678. DOI: 10.1175/JCLI-D-12-00412.1

[27] Seth A, Rauscher SA, Biasutti M, Giannini A, Camargo SJ, Rojas M. CMIP5 projected changes in the annual cycle of precipitation in monsoon regions. J Climate. 2013;26:7328-7351. DOI: 10.1175/JCLI-D-12-00726.1

[28] Trenberth KE, Dai A, Rasmussen R, Parsons D. The changing character of precipitation. Bull Am Meteor Soc. 2003;84:1205-1217. DOI: 10.1175/BAMS-84-9-1205

[29] Kharin VV, Zwiers FW. Estimating extremes in transient climate change simulations. J Climate. 2005;18:1156-1173. DOI: 10.1175/JCLI3320.1

[30] Meehl GA, Arblaster JM, Tebaldi C. Understanding future patterns of increased precipitation intensity in climate model simulations. Geophys Res Lett. 2005;32:L18719. DOI: 10.1029/2005GL023680

[31] Räisänen J. Impact of increasing CO2 on monthly-to-annual precipitation extremes: analysis of the CMIP2 experiments. Climate Dyn. 2005;24:309-323. DOI: 10.1007/s00382-004-0510-1

[32] Barnett DN, Brown SJ, Murphy JM, Sexton DMH, Webb MJ. Quantifying uncertainty in changes in extreme event frequency in response to doubled CO2 using a large ensemble of GCM simulations. Climate Dyn. 2006;26:489-511. DOI: 10.1007/s00382-005-0097-1

[33] Tebaldi C, Hayhoe K, Arblaster M, Meehl GA. Going to the extremes. Climatic Change. 2006;79:185-211. DOI: 10.1007/s10584-006-9051-4

[34] Giorgi F, Im E-S, Coppola E, Diffenbaugh NS, Gao XJ, Mariotti L, Shi Y. Higher hydroclimatic intensity with global warming. J Climate. 2011;24:5309-5324. DOI: 10.1175/2011JCLI3979.1

[35] Shiu C-J, Liu S C, Fu C, Dai A, Sun Y. How much do precipitation extremes change in a warming climate?. Geophys Res Lett. 2012;39:L17707. DOI: 10.1029/2012GL052762

[36] Scoccimarro E, Gualdi S, Bellucci A, Zampiery M, A. Navara A. Heavy precipitation events in a warmer climate: Results from CMIP5 models. J Climate. 2013;26:7902-7911. DOI: 10.1175/JCLI-D-12-00850.1

[37] Meehl GA, et al. Global climate projections. In: Climate Change 2007, The Physical Science Basis. S. Solomon, et al. Eds., Cambridge, UK, Cambridge University Press; 2007. pp. 747–845.

[38] Christensen JH, et al. Regional climate projections. In: Climate Change 2007, The Physical Science Basis. S. Solomon, et al. Eds., Cambridge, UK, Cambridge University Press; 2007. pp. 847–940.

[39] Riahi K, Gruebler A, Nakicenovic N. Scenarios of long-term socio-economic and environmental development under climate stabilization. Technol. Forecast Soc Change. 2007;74:887-935. DOI: 10.1016/j.techfore.2006.05.026

[40] Huffman G, Adler RF, Morrissey MM, Bolvin DT, Curtis S, Joyce R, McGavock B, Susskind J. Global precipitation at one-degree daily resolution from multisatellite observations. J Hydrometeor. 2001;2:36-50. DOI: 10.1175/1525-7541(2001)002,0036:GPAODD.2.0.CO;2

[41] Freychet N, Hsu H-H, Chou C, Wu C-H. Asian summer monsoon in the CMIP5 projections: A link between the change in extreme precipitation and monsoon dynamics. J Climate. 2015;28:1477-1493.

[42] Sorooshian S, Hsu KL, Gao X, Gupta HV, Imam B, Braithwaite D. Evaluation of PERSIANN system satellite based estimates of tropical rainfall. Bull Am Meteor Soc. 2000;81:2035-2046.

[43] Wu C-H, Hsu H-H, Chou M-D. Effect of the Arakan Mountains in the northwestern Indochina Peninsula on the late May Asian monsoon transition. J Geophys Res Atmos. 2014;119:10 769-10 779. DOI: 10.1002/2014JD022024

[44] Lee J-Y, Wang B. Future change of global monsoon in the CMIP5. Climate Dyn. 2014;42:101-119. DOI: 10.1007/s00382-012-1564-0

[45] Turner AG, Slingo JM. Uncertainties in future projections of extreme precipitation in the Indian monsoon region. Atmos Sci Lett. 2009;10:152-158. DOI: 10.1002/asl.223

[46] Chen C-A, Chou C, Chen C-T. Regional perspective on mechanisms for tropical precipitation frequency and intensity under global warming. J Climate. 2012;25:8487-8501. DOI: 10.1175/JCLI-D-12-00096.1

[47] Lin W, Gu W. The Eastern China flood of June 2015 and its causes. Sci Bull. 2016;61(2): 178-184.

[48] Promchote P, Wang S-YS, Johnson PG. The 2011 Great Flood in Thailand: climate diagnostics and implications from climate change. J Climate. 2016;29(1):367-379. DOI: http://dx.doi.org/10.1175/JCLI-D-15-0310.1

[49] Patankar AM, Patwardhan A, Marome WA, Porio E. Enhancing adaptation to climate change by integrating climate risk into long-term development plans and disaster management. APN E-Lib [Internet]. 2012. Available from: http://www.apn-gcr.org/resources/items/show/1572

[50] Chintraruck A, Walsh J. Bangkok and the Floods of 2011, Editor: M. Ann Miller and M. Douglass, Asia Research Institute, National University of Singapore: urban governance and the struggle for democratisation. In: Disaster Governance in Urbanising Asia. Springer, Singapore; 2016. pp. 195-209. DOI: 10.1007/978-981-287-649-2_10

[51] Lachica A P. Degraded forest rehabilitation and sustainable, forest management in East Asia region. In: APFNet Thematic Training Workshop on Degraded Forest, Rehabilitation and Sustainable Forest Management; 1–12 July 2014; 2014. pp. 79-87.

[52] Patwardhan A, Marome W. Characterizing public and private adaptation to climate change and implications for long-term adaptive capacity in Asian Megacities, APN E-Lib. 2016. Available from: http://www.apn-gcr.org/resources/items/show/1897

IntechOpen